The Fast Fourier Transform

Ben Berretta

Ian Orrell

Appalachian State University

Dr. Roshani Silwal and Dr. Zach Russell

Abstract:

This experiment investigates the spatial frequency content of diffraction patterns using a 4f optical system and computational Fourier analysis. A laser beam was directed through a slit mask and processed by two lenses performing a Fourier transform and its inverse. A CMOS camera captured images at both the Fourier and image planes. These images were processed using Fast Fourier Transforms (FFT) in *ImageJ* (8) and *OpenCV* (9), allowing for direct comparison between computational and experimentally obtained spatial frequency distributions.

To assess similarity between the experimental and simulated images, the Structural Similarity Index Measure (SSIM) was employed, yielding high similarity scores for matched slit orientations. In addition to SSIM, heat maps were generated to visually highlight local regions of similarity and difference, enhancing visual interpretation of structural alignment between each image pair. However, because SSIM scores were generally high for all comparisons, a complementary method was used to isolate frequency orientation information. The magnitude spectra of each FFT were transformed into polar coordinates to compare the angular and radial components of spatial frequency. After flattening and normalizing these polar transformed FFTs, the Pearson correlation coefficient was computed using *NumPy* (11) to quantitatively assess the similarity of orientation in the frequency structure.

The combination of these techniques; SSIM, heat map visualization, and polar Pearson correlation, provided a robust and thorough validation of the experimental data against computational predictions. The results demonstrated strong agreement between the experimental Fourier plane images and computational FFTs across all slit orientations, reinforcing the accuracy of both the optical setup and the image processing steps involving ImageJ and OpenCV. This dual method approach highlights the effectiveness of combining multiple comparison metrics when validating optical system behaviors in experimental physics.

1. Introduction

I was first motivated to study the Fast Fourier Transform due to its capabilities in music production. An example; the ability to control bass and treble separately. Bass notes are usually very low frequencies, while treble notes are usually much higher frequencies. The FFT is used to display the sound waves as frequency bands, effectively separating the bass and treble into identifiable frequencies. The FFT can also be used to analyze a wide range of frequencies; Spotify has a feature which allows the user to manipulate a large range of frequencies. Allowing the user to tune the output depending on what song is playing. The FFT is extremely applicable now, in 2025, but it is important to know where and when such an idea came from.

In the early 19th century, Jean-Baptiste Joseph Fourier (1) introduced the revolutionary concept that any complex waveform could be decomposed into a sum of simple sine and cosine functions. This discovery, known today as the Fourier series (2), has become instrumental in both theoretical and applied science. With the advent of digital computation, this idea evolved into the Fast Fourier Transform, FFT (3); a much more efficient algorithm that allows rapid transformation of time-domain signals into their frequency-domain representations. The FFT has become essential in fields ranging from signal processing and communications to quantum mechanics and astrophysics; including music production, television broadcasting, and even stellar astronomy. In all of these fields, the FFT gives insight into hidden frequency components within seemingly chaotic data.

Over the decades, FFT techniques have transformed the way scientists and engineers analyze oscillatory behavior in dynamic systems. In experimental physics, FFTs are frequently deployed to identify resonant modes; hidden frequency components within seemingly chaotic data. FFTs are also used to quantify damping and detect periodic signals obscured by noise. Applications span across disciplines, including spectroscopy (stellar astronomy), seismology (analyzing vibrations in the Earth), audio engineering (music production), and medical imaging technologies such as MRI.

In this experiment, I investigate the Fast Fourier Transform; analyzing time-domain and frequency-domain data obtained from optical systems. The aim of this paper is to reinforce the validity of FFT in experimental contexts, specifically in the field of image processing; comparing and discerning observed and computational diffraction patterns of light.

2. Theory

The Fast Fourier Transform (3) is an algorithm that efficiently computes the Discrete Fourier Transform, DFT (4), of a signal or image. Traditionally, the DFT requires $O \cdot (N^2)$ operations, where O represents the operation and N represents the number of samples. The FFT reduces this computation to just $O \cdot (N \cdot log(N))$ operations. If N = 100, the DFT requires 10,000 operations, while the FFT requires just 200 operations; a significant decrease in the number of operations, which reduces the time to compute.

In optics, the FFT is a powerful tool used for analyzing spatial frequency components. Take the Sun as an example; the FFT of sunlight produces a DFT which directly represents the spatial frequency components; the components being frequencies of light, such as visible light. The Fourier transform can be applied in many contexts, but in this experiment; when coherent light passes through an aperture or mask (a very thin slit, diameter (d) = 0.15mm), an image is formed. The image formed represents the Fourier Transform (diffraction pattern) of the aperture's function; function meaning how the physical nature of the mask affects the produced image. The image's location is referred to as the Fourier plane.

To understand how this diffraction pattern forms, it is important to view light as a wave. Light behaves as an electromagnetic wave; characterized by oscillating electric and magnetic fields. When this wavefront encounters an obstacle or aperture; such as a slit or a letter-shaped mask, it diffracts, meaning the wave bends and spreads out. As described by Huygens' principle ()5, each point along the aperture acts like a source of spherical wavelets. These wavelets interfere with each other, both constructively and destructively. The resulting interference pattern is what we observe as diffraction. This pattern contains encoded spatial frequency information, unique to

the aperture.

In the context of Fourier optics, this diffraction pattern is the Fourier Transform of the aperture. What the light wave is doing, in essence, is performing a physical Fourier Transform; redistributing its energy in space based on how it was modified by the mask. The pattern observed in the Fourier plane shows the relative contributions of different spatial frequencies. High frequency components correspond to fine details such as sharp edges and are located farther from the center of the transformed image, while low frequency components reflect broader, smoother features and are located near the center of the image.

A typical optical system used to observe the Fourier plane (diffraction pattern) is the 4f system depicted in Figure 1.

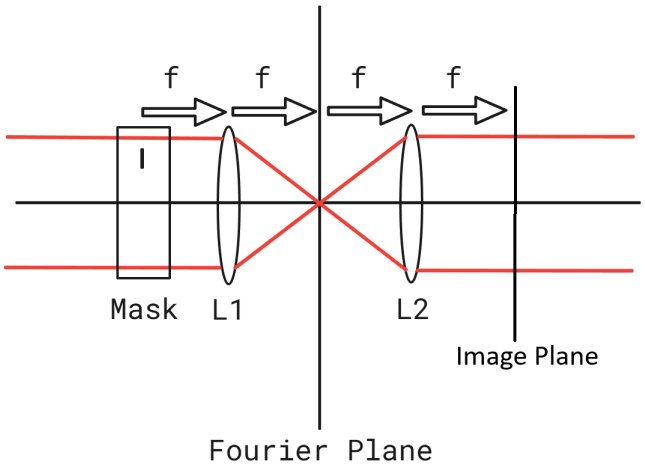

Figure 1. 4f System. From left to right, the diagram shows the mask, the Fourier transform lens (L1), and the inverse Fourier transform lens (L2). A collimated laser beam travels in a straight line, first passing through the mask, which generates a diffraction pattern representing the spatial field distribution. The first lens performs a Fourier Transform of this field, focusing its spatial frequency components at the Fourier plane, located one focal length beyond the lens. According to Snell's law (10), as the beam passes through the first lens, the change in refractive index causes the incoming parallel rays to bend; change direction. The incoming rays converge one focal length away at the Fourier plane and then continue on their path, diverging until they propagate another focal length to reach the second lens. The second lens then bends the light rays again; this time orienting them along their original path. The second lens then performs the inverse Fourier Transform, reconstructing the original field at the image plane, also positioned one focal length beyond it.

A 4f optical system consists of a mask and two lenses arranged such that the spacing between elements is determined by the focal length f of the lenses. The laser beam first passes through a mask placed one focal length in front of the first lens. It then propagates through the first and second lenses. As the laser beam enters and exits each lens, its path is influenced by the change in refractive index at the interface between air and the glass. This behavior is described by Snell's Law, which relates the angle of incidence θ_1 and the angle of refraction θ_2 to the refractive indices of the two media:

$$n_1 \sin(\theta_1) = n_2 \sin(\theta_2)$$

Here, n_1 and n_2 are the refractive indices of the incident and transmitted media, respectively. For example, when light travels from air ($n \approx 1.00$) into glass ($n \approx 1.5$), it bends toward the normal due to the higher refractive index of the lens material. The normal is an imaginary line perpendicular to the surface of the lens (glass), at the point of incidence. Refer to Figure 2 for a diagram depicting the relationship described by Snell's law.

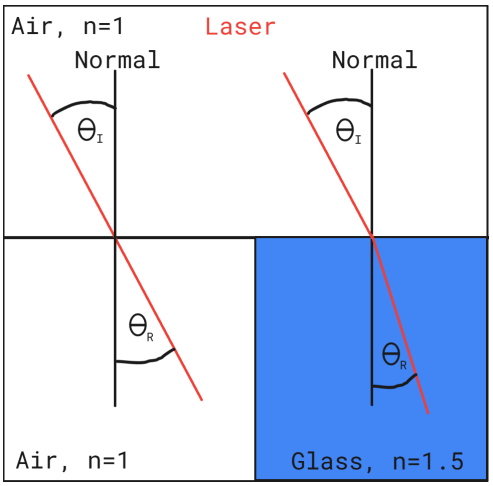

Figure 2. Illustration of Snell's Law applied to a laser beam passing from air ($n = 1.0$) into air (left) and into glass ($n = 1.5$, right). The red line represents the laser path, while the black vertical line at each boundary denotes the normal—an imaginary line perpendicular to the interface surface. The angle of incidence (θ_I) and angle of refraction (θ_R) are measured with respect to the normal. In the case of glass, the beam bends toward the normal due to the higher refractive index.

In the context of a 4f system; the beam passes through the first lens, the change in refractive index causes the incoming parallel rays to bend; change direction. The incoming rays converge one focal length away at the Fourier plane and then continue on their path, diverging until they propagate another focal length to reach the second lens. The second lens then bends the light rays again; this time orienting them along their original path. Finally, the image plane is located one focal length beyond the second lens.

This arrangement allows the first lens to perform a focused Fourier transform followed by an inverse Fourier transform performed by the second lens, effectively mapping the Fourier transform to its reconstructed image. In the end, the system produces an FFT and an inverse FFT at different locations, referred to as the Fourier plane and the image plane.

A camera can be placed in either the Fourier plane or the image plane to obtain the transformed and original images. In this experiment, images are captured in both the Fourier plane and the image plane using a CMOS camera. The Fourier plane holds information from the frequency domain, while the image plane contains the spatial representation of the object. To analyze and validate the theoretical predictions of Fourier optics, the image captured in the image plane is processed using ImageJ and OpenCV to perform a 2-D FFT. The resulting image in the frequency domain is then compared with the direct capture of the Fourier plane. Ideally, the image derived computationally via ImageJ and OpenCV should match the experimental image of the Fourier plane.

Please continue to the next page to read about the experimental procedure.

3. Experimental Procedure

The 4f system (6) is used and is depicted in Figure 1. The optical components with their specifications are listed in Table 1.

Table 1. Optical Component Specifications

Component	Specifications
4f Lens 1 (L1)	(f = 75mm)
4f Lens 2 (L2)	(f = 75mm)
Laser	(630nm-680nm, 4mw output)
CMOS Camera	(1280 x 1024 pixels)

3.1. Collimating

Figure 3 illustrates the optical setup used to straighten the beam of light. The laser beam was first aligned to travel coherently through the optical axis of the system, reflecting off two mirrors and passing through the mask and both lenses. The optical components were mounted on a rail or optical bench to ensure precise spacing and stability.

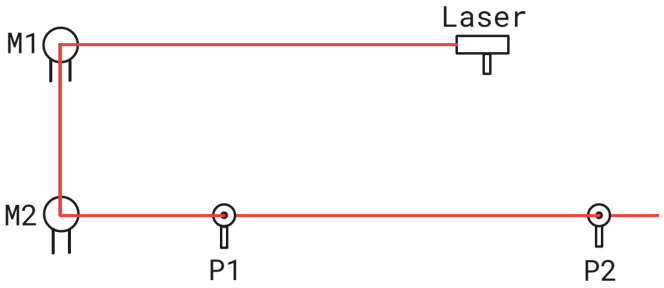

Figure 3. A collimated laser beam reflects off two adjustable mirrors, M1 and M2, allowing precise angular alignment of the beam path. After reflection, the beam passes through two pinhole filters, P1 and P2, positioned along the optical axis. The alignment of the beam through both pinholes ensures it is traveling in a straight, well-defined path for downstream optical components, such as a 4f system.

The laser was not fully uniform, and there were smudges on the lenses that added difficulties to the process. In order to properly align the laser, two adjustable pinholes are used. The pinholes, spaced 300 cm apart, are at the same height. The mirrors are adjusted until the laser passes through both pinholes. This confirmed that the laser is traveling in a straight line for 300cm, well beyond the range needed for this experiment. One of the pinholes is left in the system to increase uniformity and reduce the amount of light coming through to the mask.

Now that the laser is traveling in a straight line, the 4f system is added. The 4f system can be added at any distance downstream, as long as the light travels in a straight line through the system. When introducing the first and second lenses, they are placed at a specific distance from each other, 2f (f = 75mm). Deviations from this distance result in the laser either diverging or converging. Finding the correct locations is not difficult; the first lens is located 1f away from the mask, and the second lens is located 2f away from the first lens (3f from the mask).

Visual inspection of the beam determines that it is collimated; neither diverging nor converging. An improved collimation method would be to use a shear plate collimator; an optical tool used to accurately collimate light.

Now that the laser has been collimated, a CMOS camera is added. The camera is placed in the Fourier plane (2f from the mask) and the image plane (4f from the mask), respectively, for imaging.

3.2. Imaging

A CMOS camera (6) was used to capture images in both the Fourier plane and the image plane of the 4-F system.

Proper care was taken to ensure that the camera sensor was precisely located at the respective planes. Multiple exposures were taken to optimize contrast and sharpness. These images were later processed using ImageJ and analyzed using FFT tools in the OpenCV library.

To image the Fourier plane, the CMOS camera was placed 1f from the first lens. At this position, the lens performs a Fourier Transform of the field emerging from the mask, and the result is an intensity distribution that corresponds to the spatial frequency content of the mask. The CMOS camera was focused at this plane, and images were recorded. Unwanted diffraction patterns (noise) is blacked out using ImageJ. The final images after processing in ImageJ are depicted in Figure 4.

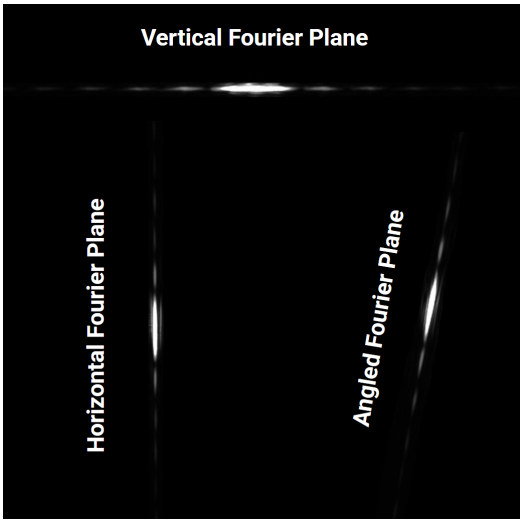

Figure 4. Direct images of the Fourier plane obtained using a CMOS sensor. Images of the Fourier plane were captured for vertical, horizontal, and angled slits. These images were cleaned using ImageJ by masking the noise using rectangular selections and grayscale conversion. OpenCV was also used to scale and align these images for structural similarity analysis (SSIM). The resulting Fourier plane images exhibit spatial frequency patterns that closely match the computational FFTs from Figure 6, both in orientation and frequency spread.

To image the image plane, the CMOS camera was repositioned to be 1f from the second lens. At this location, the system completes an inverse Fourier Transform, reconstructing the spatial field originally formed by the mask. The CMOS camera was again focused, and the image was recorded.

Furthermore, the images taken at the image plane were altered with respect to theoretical predictions. The pictures contained noisy data; blurry edges, holes in the intensity data, and off-axis diffraction patterns as discussed in the Theory section. To address the noise, ImageJ's built-in drawing tools were utilized. Using a tool that produces a clean rectangle, the images were filled in and given sharper edges. This tool was also used to remove unexpected diffraction patterns in the image. These images are depicted in Figure 5.

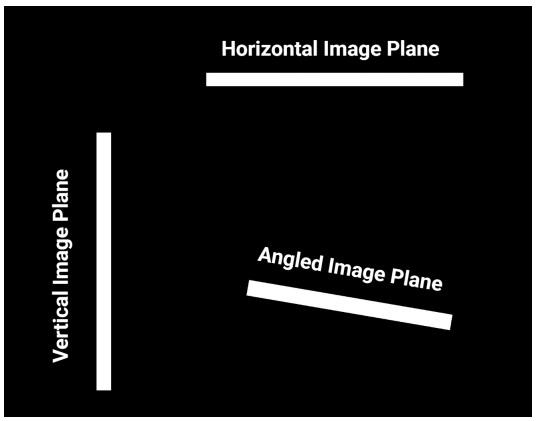

Figure 5. Three spatial domain images were captured using a slit mask oriented vertically, horizontally, and at an angle. These represent raw spatial light distributions formed at the image plane of the 4f optical system. Noise outside the region of interest was manually removed using ImageJ's rectangle selection tool, creating a uniform black background. This ensured consistency in the computational Fourier analysis by minimizing edge artifacts that would otherwise lead to off axis diffraction patterns. The images were later resized using OpenCV to a common resolution for quantitative comparison and structural similarity evaluation (SSIM). Computational FFTs of the images can be found in Figure 5.

Computational FFTs of the images in Figure 5 are obtained using ImageJ's built-in FFT image converter. These FFTs are depicted in Figure 6.

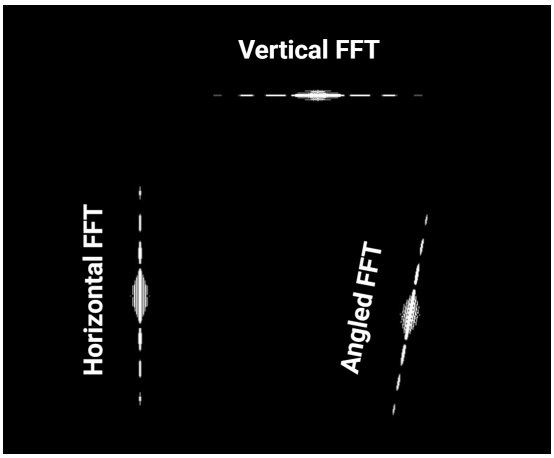

Figure 6. Fast Fourier Transforms (FFT) implemented in ImageJ were applied to each image plane configuration from Figure 4. The spatial frequency distributions are clearly aligned orthogonally to the orientation of the original slit. The vertical image produces a horizontal FFT distribution, and vice versa, while the angled slit produces a diagonally rotated frequency spectrum. All FFT outputs were centered and scaled to uniform size for fair comparison and SSIM calculation. The resulting FFTs exhibit spatial frequency patterns that closely match the Fourier plane images from Figure 4, both in orientation and frequency spread.

The capture Fourier plane images closely resemble the computational FFTs with similarities in structure, luminance and orientation. There are slight differences in structure closer to the center; computational FFTs are wider at the center, and there are slight differences in luminance further out in the spectra. These differences will have an impact when comparing the images using Structural Similarity Index Measurements (SSIMs).

4. Data Analysis and Discussion

In this experiment, I analyzed the spatial frequency content of diffraction patterns produced by a single-slit mask in a 4f optical system. Images are captured at the Fourier plane using a CMOS camera for three different slit orientations; vertical, horizontal, and angled. Each image was processed; cropping, grayscale conversion, scaling, and thresholding. The images structures were then compared using the Structural Similarity Index Measure (SSIM).

The Structural Similarity Index Measure (SSIM) is used to evaluate the similarity between two images. SSIM models are compared on the basis of changes in structural information, contrast, and luminance. It aligns very well with the observations made by the human eye and is intended to be used in conjunction; identifying image features such as orientation or spacing.

A quantitative comparison between the two images can be performed with OpenCV using the Structural Similarity Index Measure. It is based on three comparison functions, luminance (l), contrast (c), and structure (s). These three functions compare the mean values, variance, and covariance between two separate points (x and y) in the images. They are then combined in a weighted combination:

$$\mathrm{SSIM}(x,y) = l(x,y)^{\alpha} \cdot c(x,y)^{\beta} \cdot s(x,y)^{\gamma}$$

In the context of Fast Fourier Transforms, the luminance, structure, and contrast between imaged diffraction patterns in the Fourier plane and computationally derived diffraction patterns are quantitatively compared using the Structural Similarity Index Measure (SSIM). SSIM evaluates the visual similarities by analyzing local patterns (small patches) of pixel intensities. It is especially useful for assessing how closely a digitally computed FFT image resembles its experimentally captured counterpart. In this experiment, SSIM helps validate the fidelity of the optical 4f system by ensuring that structural features, such as fringe spacing, orientation, and symmetry, are preserved between the two images; the Fourier plane images are expected to closely resemble the computationally derived images. SSIM scores are recorded in Table 2. The scores are displayed as a percentage, with 100% being the most similar. The scores are around 97%, due to the similarity in the background; most of the content in the images is simply black background.

Table 2. SSIM Scores

Orientation Compared	SSIM Score (%)
Vertical Fourier plane vs vertical FFT	97.61 %
Horizontal Fourier plane vs horizontal FFT	97.56 %
Angled Fourier plane vs Angled FFT	97.30 %

Rather than comparing a single pair of images, it is more insightful to compare multiple images; comparing the vertical images to the horizontal images or the angled images. Figures 7 contains compared images, with a heat map displaying areas of similarity and difference. Comparing off orientation diffraction patterns results in lower SSIM scores; a decrease of around 2%.

The heat map is useful for visually identifying differences in the images. For a quantitative analysis, SSIM values between each pair of images can be calculated across many different orientations; showing which images are most similar to each other and which images are less similar.

In theory, images derived from identical slit orientations should exhibit the highest SSIM values due to their shared characteristics. The angled slit, due to its rotational symmetry, is expected to retain some overlap with both vertical and horizontal patterns, though to a lesser degree.

SSIM was calculated for comparisons between the captured images and their respective computational FFT images, as shown in Figure 8.

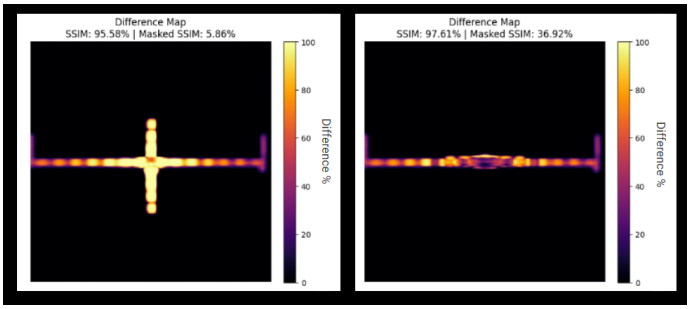

Figure 7. Both maps were generated using a custom difference heat map in Python, with masked regions emphasizing the central frequency content. These difference maps visualize the structural dissimilarity between the experimental vertical Fourier plane image and two computational FFT results. SSIM similarity scores for the image with and without a mask are displayed. The masked score simply ignores the black background, only comparing the illuminate regions of the images. On the left, the experimental image is compared to the horizontal FFT, yielding a SSIM score of 95.58%, and a masked score of 5.86%. On the right, the same experimental image is compared to the vertical FFT, resulting in a slightly higher SSIM of 97.61%, but a significantly higher masked SSIM of 36.92%, indicating greater structural alignment in the core spectral region. Visual inspection of the heat maps confirms the experimental vertical Fourier plane image is more similar to the vertical computational FFT.

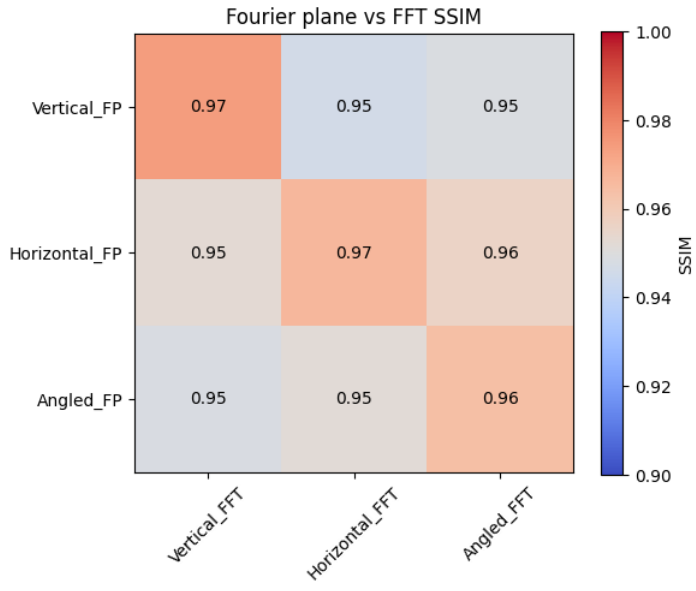

Figure 8. Pairwise SSIM score matrix comparing Fourier Plane (FP) images with their corresponding FFT images for vertical, horizontal, and angled slit orientations. Diagonal entries represent same-orientation comparisons (V_FP vs V_FFT), which yield the highest structural similarity scores. Off-diagonal entries indicate cross-orientation comparisons, where SSIM values are slightly lower due to differences in spatial frequency content.

The SSIM scores indicate that the images share similarity in their FFTs. This result is consistent with theoretical expectations, since the FFT of a single slit approximates a sine function perpendicular to the slit's orientation and this is observed in both the captured images and computed images. A vertical slit produces horizontal frequency bands and a horizontal slit produces vertical bands. An angled slit results in a rotated diffraction pattern, which essentially produced a mirror image.

The SSIM matrix reveals that the highest similarity scores occur along the diagonal, where each Fourier Plane (FP) image is compared with its corresponding FFT image of the same slit orientation. This confirms that the structural characteristics of the diffraction patterns are best preserved within matched pairs.

However, off-diagonal comparisons between mismatched orientations (vertical FP with horizontal FFT) result in noticeably high SSIM values, around 0.94-0.96. This result can be expected due to the similarities in the black background, but not to this degree. The off-diagonal scores are expected to be closer to 0.90-0.93.

Instead of comparing luminance, structure, and contrast, the orientation of the images, the angular information can be directly compared. This method is particularly effective for diffraction patterns, where spatial frequency orientation carries significant meaning.

Each pixel in the FFT magnitude image represents a specific spatial frequency; its distance from the center corresponds to the magnitude of the frequency, and its angle from the center defines the direction (orientation) of that frequency in the original image. Each pixel location and magnitude on the images is remapped from Cartesian coordinates (u, v) to polar coordinates (ρ, θ). In this context, the radial coordinate ρ represents the frequency magnitude, while the angular coordinate θ encodes the orientation of those frequencies.

After converting both the experimental and computational FFT images into polar coordinates, the resulting images are flattened and normalized. The NumPy "np.corrcoef" function (11) used to compare the images requires flattening, and normalization removes any intensity bias. Flattening allows the comparison to function and normalization enables a more direct comparison of orientation. The Pearson correlation coefficient r (7) is computed for all combinations of images. Values range from 0-1, close to 1 indicating strong agreement across both radial and angular components. Figure 9 displays the scores in a pairwise grid.

High correlation values suggest strong agreement between the orientation of captured images and their respective computational models. Diagonal entries represent same orientation comparisons, which yield the highest structural similarity scores. Off-diagonal entries indicate cross-orientation comparisons, where scores are lower due to differences in spatial frequency orientation; with the exception of the angled and horizontal comparisons. Visual inspection of the images in Figures 3 and 5 confirms that the orientations of the angled and horizontal images are similar and high Pearson correlation coefficient scores are expected.

Two complementary quantitative techniques were employed; the Structural Similarity Index Measure (SSIM) and the Pearson correlation coefficient. SSIM provided a metric sensitive to luminance, contrast, and local structure, making it well suited for comparing image textures and intensity patterns. In parallel, the Pearson correlation coefficient, computed between flattened polar FFT magnitude information, offered a simpler perspective by capturing similarities in orientations. High SSIM values indicated visual similarity in spatial content, while strong Pearson correlation

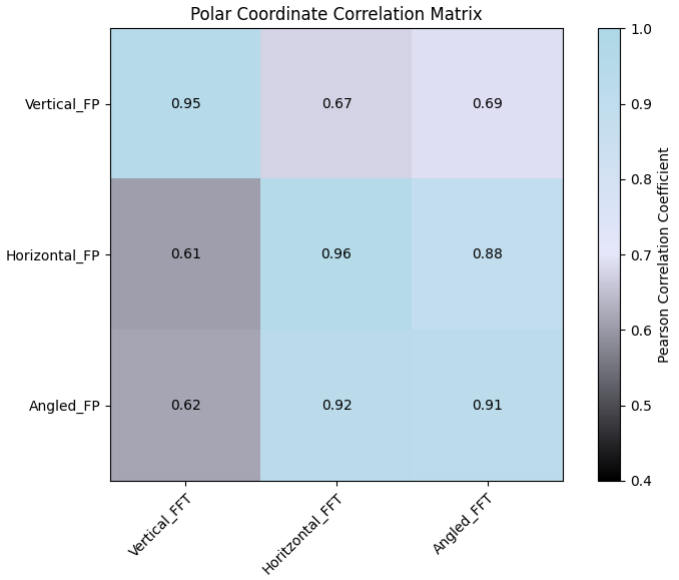

Figure 9. Pairwise Pearson correlation coefficient score matrix comparing flattened and normalized Fourier Plane (FP) images with their corresponding flattened and normalized FFT images for vertical, horizontal, and angled slit orientations. Diagonal entries represent same-orientation comparisons (V_FP vs V_FFT), which yield the highest structural similarity scores. Off-diagonal entries indicate cross-orientation comparisons, where scores are lower due to differences in spatial frequency orientation.

values confirmed agreement in image orientation. The combination of these methods enabled robust evaluation and validation of the computational FFT. Together, they provide compelling evidence that the experimentally observed diffraction patterns are consistent with the computational FFT models, reinforcing the validity of both the optical system and the simulated transforms.

5. Conclusion

This experiment demonstrated a robust approach to validating the spatial frequency content of diffraction patterns captured using a 4f optical system. By imaging both the Fourier and image planes for multiple slit orientations and applying computational Fourier analysis using ImageJ and OpenCV, strong agreement was found between experimentally captured diffraction patterns and computationally derived FFTs.

Multiple analytical techniques were deployed to rigorously assess similarity. The Structural Similarity Index Measure (SSIM) was used to quantify visual similarity based on luminance, contrast, and structural content, revealing consistently high similarity scores between matched orientations. To visually assess similarity, heat maps were generated to localize areas of similarity and difference. Recognizing the limitations of SSIM in cases with uniform backgrounds, the analysis was extended by transforming FFT magnitude spectra into polar coordinates, isolating frequency orientation from luminance content. These polar-transformed images were flattened and normalized, enabling direct comparison of orientation using the Pearson correlation coefficient. The correlation scores reinforced the SSIM results, showing high correlation for same-orientation pairs and lower correlation for mismatched orientations.

Together, these techniques formed a multifaceted approach to verifying the Fast Fourier Transform. The strong alignment across SSIM, heat maps, and polar Pearson correlation confirmed the fidelity of both the optical system and the computational methods used. This comprehensive comparison not only validated the experimental data but also highlights the power of combining multiple metrics when assessing the fidelity of traditional optical physics and modern image processing tools.

6. Appendix

6.1. Derivations

6.1.1. Derivation of the Fast Fourier Transform (FFT)

The DFT of a sequence x_n of length N is defined as:

$$X_k = \sum_{n=0}^{N-1} x_n \, e^{-2\pi i k n/N}, \quad k = 0, 1, ..., N-1.$$

This direct computation requires $\mathcal{O}(N^2)$ operations. The FFT reduces this to $\mathcal{O}(N \log N)$ by exploiting symmetries in the exponential terms and applying a divide-and-conquer strategy.

Assume N is even. The input sequence x_n can be split into two halves — one consisting of the even-indexed terms and the other of the odd-indexed terms:

$$x_n = \begin{cases} x_{2n} & \text{(even indices)} \\ x_{2n+1} & \text{(odd indices)} \end{cases}$$

Substituting into the DFT definition:

$$X_k = \sum_{n=0}^{N/2-1} x_{2n} e^{-2\pi i k(2n)/N} + \sum_{n=0}^{N/2-1} x_{2n+1} e^{-2\pi i k(2n+1)/N}.$$

Factor out the exponentials:

$$X_k = \sum_{n=0}^{N/2-1} x_{2n} e^{-2\pi i k n/(N/2)} + e^{-2\pi i k/N} \sum_{n=0}^{N/2-1} x_{2n+1} e^{-2\pi i k n/(N/2)}.$$

Define two smaller DFTs:

$$E_k = \sum_{n=0}^{N/2-1} x_{2n} e^{-2\pi i k n/(N/2)}, \quad O_k = \sum_{n=0}^{N/2-1} x_{2n+1} e^{-2\pi i k n/(N/2)}.$$

Thus, the DFT becomes:

$$X_k = E_k + W_N^k O_k,$$
$$X_{k+N/2} = E_k - W_N^k O_k,$$

where $W_N^k = e^{-2\pi i k/N}$ is the twiddle factor, capturing the phase shift between even and odd components.

This recursive formulation divides a size-N DFT into two size-$N/2$ DFTs, which are further divided until reaching the smallest possible size: the **base case**.

The recursion terminates when the sequence length N is 1; this is the **base case**, where the DFT of a single point is simply the point itself: $X_0 = x_0$.

The assumption that N is a power of 2 (i.e., $N = 2^m$) is crucial because it ensures that the sequence can be evenly halved at each recursive level. This guarantees that the total number of operations scales as:

$$\mathcal{O}(N \log N)$$

rather than $\mathcal{O}(N^2)$, providing a significant speed advantage for large datasets. This efficiency gain makes the FFT fundamental to modern signal and image processing, including applications in Fourier optics, audio analysis, and data compression.

6.1.2. Structural Similarity Index (SSIM) Derivation

The Structural Similarity Index Measure (SSIM) is a perceptual metric that evaluates image similarity by comparing luminance, contrast, and structure between two corresponding image patches. Given two image patches x and y, the SSIM score is defined as:

$$\text{SSIM}(x, y) = [l(x, y)]^{\alpha} \cdot [c(x, y)]^{\beta} \cdot [s(x, y)]^{\gamma}$$

where:

- $l(x, y)$ is the luminance comparison function,
- $c(x, y)$ is the contrast comparison function,
- $s(x, y)$ is the structure comparison function,
- α, β, and γ are parameters to adjust the relative importance of each component (typically all set to 1).

Luminance Comparison Luminance compares the mean intensity values of the two patches:

$$l(x, y) = \frac{2\mu_x\mu_y + C_1}{\mu_x^2 + \mu_y^2 + C_1}$$

where μ_x and μ_y are the mean pixel values of x and y, respectively, and C_1 is a small constant to avoid division by zero.

Contrast Comparison Contrast compares the standard deviations (or variance) of the two patches:

$$c(x, y) = \frac{2\sigma_x\sigma_y + C_2}{\sigma_x^2 + \sigma_y^2 + C_2}$$

where σ_x and σ_y are the standard deviations of x and y, and C_2 is another stabilizing constant.

Structure Comparison Structure compares the normalized correlation between the two patches:

$$s(x, y) = \frac{\sigma_{xy} + C_3}{\sigma_x\sigma_y + C_3}$$

where σ_{xy} is the covariance between x and y, and $C_3 = C_2/2$ by convention.

Final SSIM Formula Assuming $\alpha = \beta = \gamma = 1$, the full SSIM index simplifies to:

$$\text{SSIM}(x, y) = \frac{(2\mu_x\mu_y + C_1)(2\sigma_{xy} + C_2)}{(\mu_x^2 + \mu_y^2 + C_1)(\sigma_x^2 + \sigma_y^2 + C_2)}$$

This formula is computed locally over image patches and then averaged over the entire image to produce a global SSIM score.

6.1.3. Derivation of the Pearson Correlation Coefficient

The Pearson correlation coefficient r measures the linear relationship between two variables X and Y. It is defined as the normalized covariance between them:

$$r = \frac{\text{cov}(X, Y)}{\sigma_X \sigma_Y}$$

Covariance quantifies how much two variables vary together and is given by:

$$\text{cov}(X, Y) = \frac{1}{n} \sum_{i=1}^{n} (x_i - \bar{x})(y_i - \bar{y})$$

where:

- x_i, y_i are the individual observations,
- $\bar{x}, \bar{y}$ are the sample means of X and Y,
- n is the total number of paired observations.

The standard deviations of X and Y are given by:

$$\sigma_X = \sqrt{\frac{1}{n} \sum_{i=1}^{n} (x_i - \bar{x})^2}, \qquad \sigma_Y = \sqrt{\frac{1}{n} \sum_{i=1}^{n} (y_i - \bar{y})^2}$$

Substituting the covariance and standard deviations into the definition of r, we get:

$$\begin{aligned} r &= \frac{\frac{1}{n} \sum_{i=1}^{n} (x_i - \bar{x})(y_i - \bar{y})}{\sqrt{\frac{1}{n} \sum_{i=1}^{n} (x_i - \bar{x})^2} \cdot \sqrt{\frac{1}{n} \sum_{i=1}^{n} (y_i - \bar{y})^2}} \\ &= \frac{\sum_{i=1}^{n} (x_i - \bar{x})(y_i - \bar{y})}{\sqrt{\sum_{i=1}^{n} (x_i - \bar{x})^2} \cdot \sqrt{\sum_{i=1}^{n} (y_i - \bar{y})^2}} \end{aligned}$$

This final expression shows that Pearson's r is a dimensionless quantity bounded between -1 and 1, reflecting the strength and direction of a linear relationship between X and Y.

6.2. Helpful people

Lab partner: *Ian Orrell*
Lab instructors: *Dr. Roshani Silwal, Dr. Zach Russell*

6.3. Helpful resources

Google Colab for graphing the data. It has many built in libraries (OpenCV (9)) and a built in AI to help understand the code better.

ChatGPT 4o for formatting my sources to APA style and finding information on the FFT and possible comparison methods.

Overleaf's built-in grammar correction tool. This also gives suggestions for better vocabulary.

AutoDraw for making diagrams such as Figure 1 and 2.

References

[1] American Physical Society. (2010, March). *This Month in Physics History: March 21, 1768: Birth of Jean-Baptiste Joseph Fourier*. APS Archives. Retrieved from https://www.aps.org/archives/publications/apsnews/201003/physicshistory.cfm

[2] Sanderson, G. (2017, July). *But what is a Fourier series? From heat flow to circle drawings | DE4* [Video]. 3Blue1Brown. Retrieved from https://www.youtube.com/watch?v=spUNpyF58BY

[3] Wikipedia. (2023). *Fast Fourier transform*. Retrieved from https://en.wikipedia.org/wiki/Fast_Fourier_transform

[4] Wikipedia. (2023). *Discrete Fourier transform*. Retrieved from https://en.wikipedia.org/wiki/Discrete_Fourier_transform

[5] BYJU'S. (n.d.). *Huygens principle and diffraction*. Retrieved April 15, 2025, from https://byjus.com/physics/the-huygens-principle-and-the-principle-of-a-wave-front/#:~:text=called%20a%20wavefront.-,Huygens%20Principle%20and%20Diffraction,form%20of%20a%20circular%20wavefront.

[6] Optics for Hire. (2020, August 5). *4F optical system in Fourier optics*. Retrieved April 15, 2025, from https://www.opticsforhire.com/blog/4f-optical-system-fourier-optics/

[7] Pearson correlation coefficient. (n.d.). *Wikipedia*. Retrieved April 18, 2025, from https://en.wikipedia.org/wiki/Pearson_correlation_coefficient

[8] Schneider, C. A., Rasband, W. S., Eliceiri, K. W. (2012). *NIH Image to ImageJ: 25 years of image analysis*. Nature Methods, 9(7), 671–675. https://imagej.net/ij/ https://doi.org/10.1038/nmeth.2089

[9] Bradski, G. (2000). *The OpenCV Library*. Dr. Dobb's Journal of Software Tools. Retrieved from https://opencv.org/

[10] Chu, K. (n.d.). *Snell's Law*. University of British Columbia. Retrieved April 18, 2025, from https://personal.math.ubc.ca/~cass/courses/m309-01a/chu/Fundamentals/snell.htm

[11] NumPy Developers. (2024). *numpy.corrcoef*. NumPy v2.2 Manual. Retrieved April 18, 2025, from https://numpy.org/doc/2.2/reference/generated/numpy.corrcoef.html

[12] Born, M., & Wolf, E. (n.d.). *Principles of optics* [PDF file]. Retrieved from https://cdn.preterhuman.net/texts/science_and_technology/physics/Optics/Principles%20of%20Optics%20-%20M.Born,%20E.%20Wolf.pdf

[13] Taylor, J. R. (1997). *An introduction to error analysis: The study of uncertainties in physical measurements* (2nd ed.). Sausalito, CA: University Science Books. Retrieved from https://asulearn.appstate.edu/pluginfile.php/6535438/mod_resource/content/1/Error%20Analysis%20Textbook.pdf

[14] Muller, D. (2020, August). *The most beautiful equation in math* [Video]. Veritasium. Retrieved from https://www.youtube.com/watch?v=r6sGWTCMz2k

[15] Sanderson, G. (2018, January). *What is the Fourier Transform? Visualizing the frequency domain* [Video]. 3Blue1Brown. Retrieved from https://www.youtube.com/watch?v=nmgFG7PUHfo

[16] Wikipedia. (2023). *Fourier transform*. Retrieved from https://en.wikipedia.org/wiki/Fourier_transform

[17] NTi Audio. (n.d.). *Fast Fourier Transform (FFT) explained*. Retrieved from https://www.nti-audio.com/en/support/know-how/fast-fourier-transform-fft

[18] Hamming, A. (2022, November). *Why we use the DFT - Introduction to FFT (with animation)* [Video]. Retrieved from https://www.youtube.com/watch?v=kBZMnEYg24w

[19] STEM Learning Center. (2021, February). *Fourier series and phasors explained* [Video]. Retrieved from https://www.youtube.com/watch?v=E2D6DRkmXd4

6.4. Links

Code
Lab Notebook
AutoDraw

The Faraday Effect ☻

Contact via email or text:
berrettabt@appstate.edu
benberretta@gmail.com
980-254-4909